Quantum Electronics **50** (8) 793–800 (2020)

LASER MEDICINE

https://doi.org/10.1070/QEL17226

Heat transfer in water under laser heating through fibres for endovenous laser coagulation

V.P. Minaev, N.V. Minaev, V.Yu. Bogachev, K.A. Kaperiz, D.A. Fedorov, V.I. Yusupov

Abstract. **We report the results of studying heat transfer in water heated by a cw laser with wavelengths of 1.55 and 1.94 μm through optical fibres with end-face and radial outputs. It is shown that, depending on the power and wavelength of the radiation, heat transfer is implemented via convection, bubble boiling, or explosive boiling and occurs asymmetrically, mainly in the forward–upward direction for the fibre with the end-face output and upward for the radial output.**

Keywords: *laser heating of water, heat transfer, convection, explosive boiling, endovenous laser coagulation.*

1. Introduction

The use of laser heating of liquids for obliteration of varicose veins (endovenous laser coagulation, EVLC) [1] and treatment of cysts of various localisation [2] has become widespread over the past two decades (this is especially true for EVLC). This process is facilitated by the high efficiency of laser technologies that possess low invasiveness, reduced pain and occurrence of postoperative complications. To implement the method, laser radiation with different wavelengths (from 0.45 to 1.94 μm) is used. Initially, fibres were used for EVLC with the output of radiation through the end face of the fibre. Such fibres are still used by phlebologists. Their advantages are the low cost and the possibility of reuse after repeated sterilisation.

Since the main mechanism that triggers the fibrous transformation in EVLC is thermal damage to the vein wall (see, e.g., [1]), the procedure also uses more expensive optical fibres in which radiation is coupled out in the radial direction perpendicular to the fibre axis (the so-called radial optical fibres). They are considered to provide more uniform illumination of the vein wall. Discussions are ongoing on the selection of optimal instruments and treatment parameters using laser radiation.

Optimisation essentially relies on the understanding of the processes that occur during EVLC. In this regard, issues of mathematical and physical modelling of such processes are undoubtedly relevant [3–8]. An important aspect is heat transfer processes. At present, the most popular opinion is that the main role in heat transfer is played by boiling of water at the exit from the fibre, which gives rise to jets consisting of water and gas-vapour microbubbles [9]. In Ref. [9] a study was carried out based on sonograms obtained using ultrasound devices; however, these sonograms are not sufficiently informative and allow ambiguous interpretation [10]. In this regard, in the present work we experimentally investigate the dynamics of water heating induced by cw laser radiation with wavelengths of 1.55 and 1.94 μm, the most popular so-called 'water-absorbed' range. These wavelengths are characterised by the predominance of absorption of radiation by water over absorption by haemoglobin. In this case, experimental modelling of laser-induced hydrodynamic processes occurring in the blood can be carried out in water with registration of the heating process by the shadow optical method.

2. Materials and methods

As radiation sources, LSP-'IRE-Polyus' devices based on fibre lasers (wavelength $\lambda = 1.55$ μm, power $P = 15$ W and $\lambda = 1.94$ μm, and $P = 10$ W) were used. When choosing the radiation power, it was taken into account that in the case of fibres with a radial output of radiation in the practice of using EVLC in the First Phlebology Centre, the typical power values are 8–10 W for 1.55 μm, and 4–5 W for 1.94 μm. Two configurations of the experimental setup were used: for recording the shadow image perpendicular to the axes of the optical fibres (Fig. 1a) and along them (Fig. 1b). Optical recording was carried out by a Fastcam SA3 high-speed camera (Photron, USA) using backlight (shadow method) with a rate of 4000 frames per second and a frame duration of 20 μs. In the experiments, optic fibres intended for EVLC were used with end-face (core diameter 0.6 mm) and radial radiation outputs (Biolitec, Germany). The diameter of the protective bulb of the radial-output fibre was 1.85 mm. Methods for outcoupling radiation are schematically shown in Fig. 1c. A shell with a valve from a 6F introducer (Balton, Poland) was used to enter the fibre into a cell with water. To register

V.P. Minaev IRE-Polyus Scientific and Technical Association, pl. Akad. Vvedenskogo 1/3, 141190 Fryazino, Moscow region, Russia;
N.V. Minaev, V.I. Yusupov Federal Scientific Research Centre 'Crystallography and Photonics', Russian Academy of Sciences, Institute of Photon Technologies, ul. Pionerskaya 2, 108840 Moscow, Troitsk, Russia; e-mail: minaevn@gmail.com;
V.Yu. Bogachev Pirogov Russian National Research Medical University, ul. Ostrovityanova 1, 117997 Moscow, Russia;
K.A. Kaperiz OOO First Phlebology Centre, ul. Dmitrya Ulyanova 31, 117447 Moscow, Russia;
D.A. Fedorov Niarmedik Clinic, ul. Gagarina 37B, 249034 Obninsk, Kaluga region, Russia

Received 13 December 2019; revision received 30 January 2020
Kvantovaya Elektronika **50** (8) 793–800 (2020)
Translated by V.L. Derbov

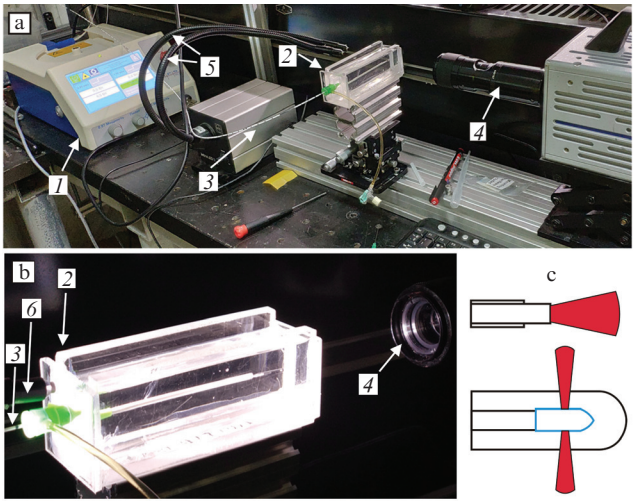

Figure 1. (a) Experimental setup for video recording perpendicular to the fibre, (b) cell with water for video recording along the fibre and (c) schematic representation of laser radiation at the exit from the end-face and radially emitting optical fibres: (*1*) laser source; (*2*) cell; (*3*) optical fibre; (*4*) high-speed camera; (*5*) background illumination; (*6*) fibre introducing device.

broadband acoustic signals at a distance of ~3 cm from the end of the laser fibre, an 8103 hydrophone (Bruhl and Kjepr, Denmark) was installed with a recording band of 0.1 Hz–200 kHz and a sensitivity of –211 dB per 1 V μPa^{-1}.

3. Experimental results

3.1. Optical fibre with end-face output of radiation

Wavelength λ = 1.55 μm. Figure 2 shows high-speed video recording frames of shadow patterns in the process of heating water by radiation with $\lambda = 1.55$ μm at $P = 5$ W. It is seen that heat transfer in this case is due to convection. After 32 ms, a gradient wave-like structure is formed in water near the lower part of the fibre end face, which gradually expands in the upward–forward direction. The velocity of the heat front in the vertical direction is about 16 mm s^{-1}; after about 0.2 s, stationary heat transfer is established in the upward–forward direction.

As the radiation power increases to 12 W, the scenario changes (Fig. 3). To make video recording more informative, the time intervals between frames change depending on the variation speed of shadow patterns. During the first 825 ms, as with a power of 5 W, convective heat transfer is observed, but with more pronounced heat front gradients. The velocity of the front in the vertical direction is about 20 mm s^{-1}. In contrast to the case of $P = 5$ W, approximately 0.82 s after the radiation is applied, explosive boiling of water at the end face occurs with the formation of a bubble with a diameter of about 5 mm. The time of bubble formation and collapse is about 1 ms.

After the collapse of the macrobubble, about 50 ms later, a relatively long-lived stationary pulsing vapour-gas bubble

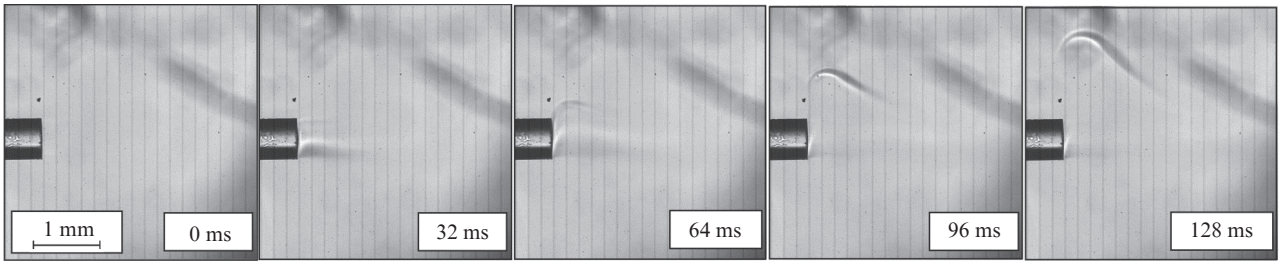

Figure 2. Dynamics of water heating by laser radiation with $\lambda = 1.55$ μm and $P = 5$ W (time from the moment of radiation onset is indicated).

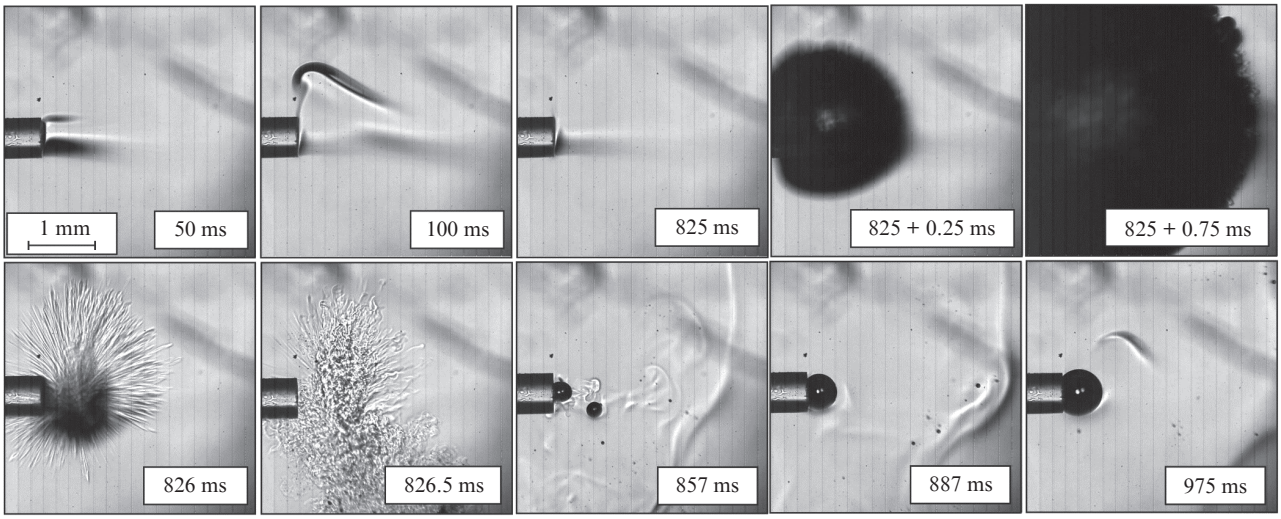

Figure 3. Dynamics of water heating by laser radiation with $\lambda = 1.55$ μm and $P = 12$ W.

with sharp boundaries with a diameter slightly exceeding the diameter of the fibre (0.6 mm) forms at the fibre end face. Water is heated at the bubble boundary, as evidenced by the appearance in the frame corresponding to 975 ms of an image of a thermal front propagating up and down.

The heating option with explosive boiling events is not the only possible scenario. Figure 4 shows the dynamics of water heating by radiation with $\lambda = 1.55$ μm and $P = 15$ W. During the first 0.5 s, convection heat transfer occurs in the upward--forward direction. Near the lower part of the end face of the fibre, a darkening corresponding to the temperature gradient is observed. This process ends with the beginning of the formation of a vapour-gas bubble with sharp boundaries at a distance of about 0.5 mm from the fibre end, closer to its lower part. Within 2 ms, the diameter of the bubble rapidly increases to about 1.2 mm, after which, with virtually no change in volume, its shape begins to change.

Note that in this case, explosive boiling does not occur. After about 0.87 s, the bubble detaches from the end of the fibre and begins to move forward and upward. Its shape changes, and the volume decreases due to condensation of the steam with the transfer of heat to the surrounding water. At the same time, a new bubble forms and grows at the fibre end face with sharp boundaries, at the boundary of which water is heated with convective heat transfer upstream. Subsequently, the bubble sizes vary within 0.5–1.2 mm.

Thus, the presented results show that, with the exception of the collapse of a vapour-gas bubble formed as a result of explosive boiling at $P = 12$ W, no significant downward heat transfer is observed.

The wavelength $\lambda = 1.94$ μm. When using radiation with $\lambda = 1.94$ μm, due to the stronger absorption of radiation in water, thermal phenomena are observed at lower powers than in the case of radiation with $\lambda = 1.55$ μm.

Figure 5 shows the high-speed video frames when water is heated by radiation with a power of $P = 1$ W. The first frame shows that, as expected, heat is released at the output end face of the fibre in a thin layer about 0.2 mm thick. 38 + 0.25 ms after the onset of radiation, explosive boiling at the end of the fibre forms a vapour-gas macrobubble with a diameter of about 2 mm. After another 0.25 ms, the bubble collapses with the ejection of a 'jet' of microbubbles forward and flows of heated water in all directions. In this case, the expansion rate of the bubble is about 4 m s^{-1}. After this, a pulsating vapour-gas bubble with sharp boundaries begins to grow at the output end of the fibre in about 1.5 ms, the size of which reaches the diameter of the fibre. From the bubble a convective heat flow moves upward. Shadow photography frames do not detect downward heat flux.

Figure 6 shows the dynamics of the shadow pattern of water heating at $P = 2$ W. In this case, explosive boiling with the formation and collapse of a gas-vapour bubble occurs earlier – after about 12.5 ms. The bubble expansion rate is also about 4 m s^{-1}. In this case, a bubble is ejected forward, which transforms into a jet consisting of heated water and microbubbles that condense after about 1 ms. Then, for about 10 ms, near the end of the fibre, boiling occurs with the for-

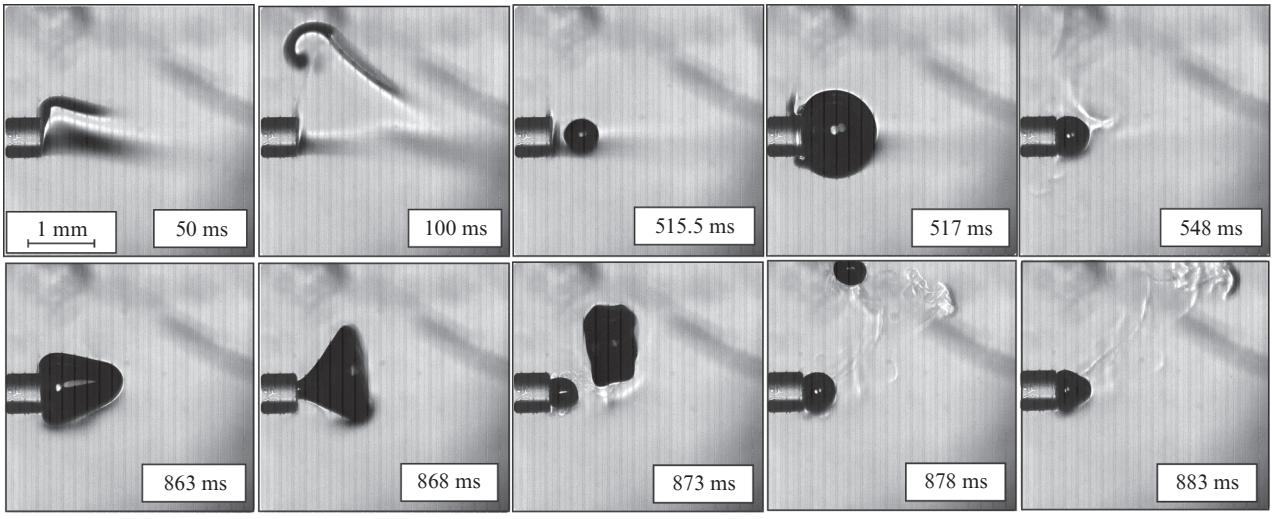

Figure 4. Dynamics of water heating by laser radiation with $\lambda = 1.55$ μm and $P = 15$ W.

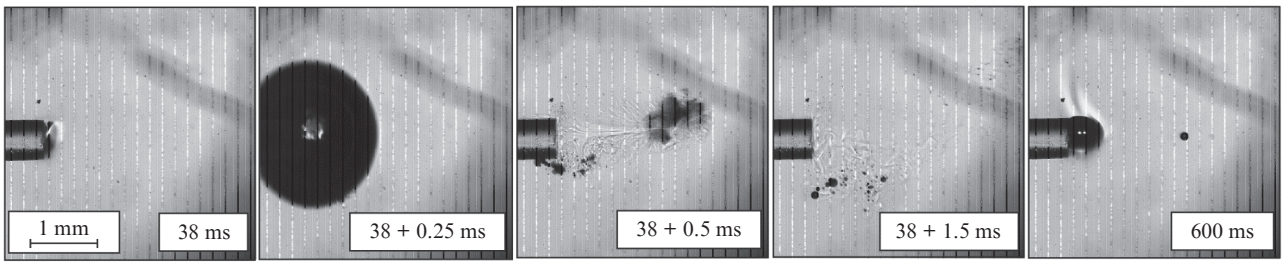

Figure 5. Dynamics of water heating by laser radiation with $\lambda = 1.94$ μm and $P = 1$ W.

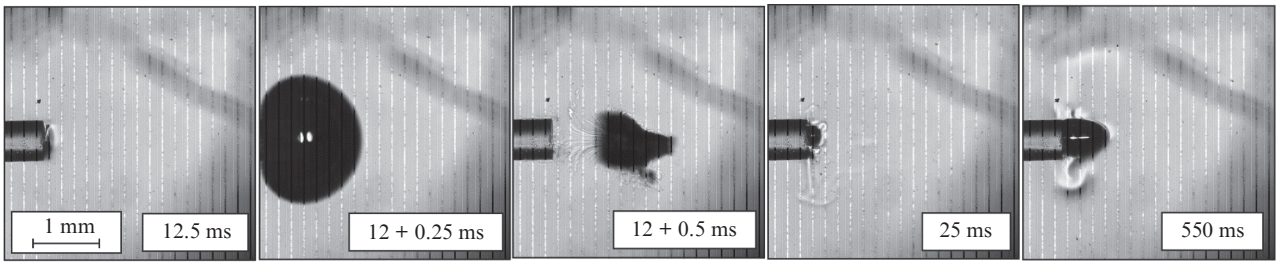

Figure 6. Dynamics of water heating by laser radiation with $\lambda = 1.94$ μm and $P = 2$ W.

mation and collapse of bubbles 0.1 – 0.2 mm in diameter. Further, during the entire recording time (0.5 s), a pulsating vapour-gas bubble with a diameter slightly less than 1 mm with sharp boundaries exists at the end of the fibre. From this bubble, as with a power of $P = 1$ W, convective flux predominantly moves forward and upward.

Similar, but more intense processes occur at a radiation power of $P = 3$ W. During the first 0.3 s of observation, four vapour-gas macrobubbles 1.5 – 2 mm in diameter have time to form and collapse with the ejection of jets (after 7.5 ms, 55 ms, 0.21 s and 0.28 s after the radiation is turned on). In this case, a pulsating bubble with sharp boundaries is retained at the end face of the fibre most of the time, from which heat flows in the surrounding water. Before the formation of the macrobubble, the pulsating bubble comes off, and a heated layer of water remains at the end. When a macrobubble collapses, part of it breaks away and moves forward, transforming into a jet of microbubbles. After the macrobubble collapses for about 3 ms, boiling water is observed at the end face with formation and collapse of bubbles less than 0.3 mm in size. After that, approximately in 7 ms a long-lived pulsating bubble with a diameter of about 1 mm forms, which exists until the next event of explosive boiling with formation and collapse of a macrobubble.

3.2. Optical fibre with radial output

Wavelength $\lambda = 1.55$ μm. Figure 7 shows the sequence of high-speed video frames when water is heated by laser radiation with $\lambda = 1.55$ μm and $P = 15$ W, through a radial-output fibre. The results showed that when using a radial-output fibre with radiation powers up to 15 W, water is heated by convection. In this case, the heat transfer is directed mainly upward. For ~0.3 s, a stable area of heated water is formed below the fibre, the heat from which (as in the case of the end-face output of the radiation) does not propagate downward, but judging by the video frames, it convectively 'flows up'. Full-face video recording (towards the fibre) does not allow a clear picture of heat transfer; nevertheless, it can be recognised that heat convectively propagates upward in an angle slightly larger than 90°.

Wavelength $\lambda = 1.94$ μm. When using radial optical fibres and radiation with $\lambda = 1.94$ μm, the processes of effective heat transfer begin at lower power levels. Figure 8 shows the high-speed photography frames, made in profile and full-face, characterising the dynamics of water heating by laser radiation with a power of $P = 5$ W until the onset of explosive boiling. The images in the figure demonstrate heat transfer due to convection in the upward direction with the velocity of the heat wave front from 7 to 14 mm s^{-1}.

However, in contrast to the use of radiation with $\lambda = 1.55$ μm, already in less than a second (in experiments from 0.5 to 0.9 s), an explosive boiling occurs after the radiation is turned on. As a result, a vapour-gas macrobubble is formed (Fig. 9), which then collapses within ~1 ms with the formation of an expanding cloud of vapour-gas microbubbles.

Then, after an explosive boiling act, a fine-bubble boiling begins on the surface of the fibre, in which numerous pulsating bubbles with sharp boundaries form around the perimeter of the radiation exit (Fig. 10). Near the bubbles heat fluxes are formed, directed upward (mainly) and to the sides. In the process of boiling, part of the bubbles detaches from the fibre, and some of them collapse upon reaching a size of about 0.5 mm, throwing out heated 'prominences'. Thus, most of the time, small-bubble boiling prevails, which forms heat fluxes directed mainly upward with periodically occurring

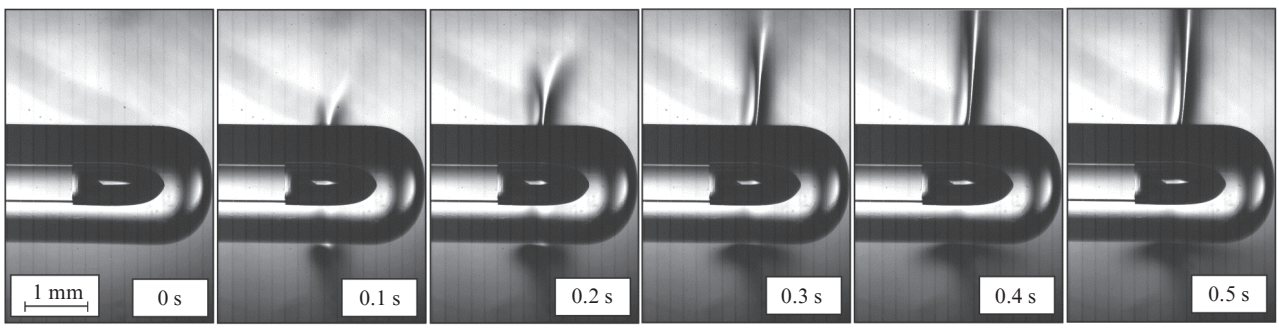

Figure 7. Dynamics of water heating by laser radiation with $\lambda = 1.55$ μm and $P = 15$ W through a radial fibre. The video recording was perpendicular to the axis of the fibre (in profile).

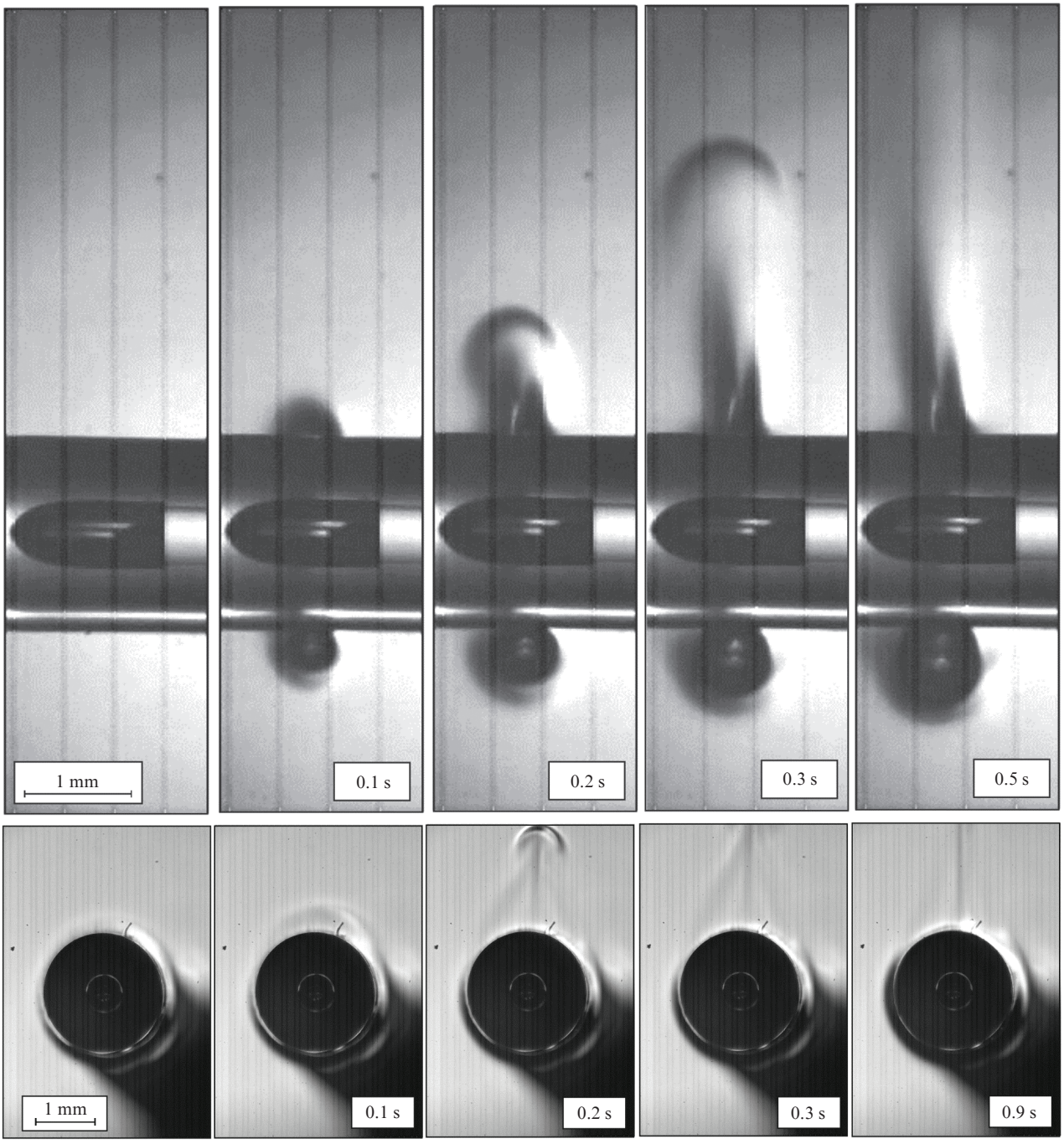

Figure 8. Dynamics of water heating through a fibre with radial output by laser radiation with $\lambda = 1.94$ μm and $P = 5$ W before the beginning of explosive boiling (the upper row is a profile view, and the lower row is a full-face view).

explosive boiling events, while part of the heat flux is directed downward.

In this experiment, sound was additionally recorded using a broadband hydrophone immersed in water. Figure 11 shows the portion of the acoustic signal corresponding to the moment of the first explosive boiling, and its spectrum. A burst is released on the signal recording, which decays over a time of ~2 ms; in front of it one can observe a chain of short pulses, the maximum amplitudes of which gradually increase with time. Peaks in the 2×10^3, 2×10^4, and 3×10^5 Hz regions are distinguished against the broadband spectrum.

4. Discussion of results

The experiments showed that the dynamics of water heating by cw laser irradiation is largely determined by both the type of optical fibres used (end-face or radial output) and the radiation wavelengths ($\lambda = 1.55$ and 1.94 μm). The first circumstance is obviously associated with different geometry of the output of laser radiation into water, and the second, with a difference in absorption coefficients. The thickness of the layer in which radiation is absorbed in the blood in the process of EVLC is determined by the effective attenuation coefficient μ_{eff}, which, in addition to absorption, takes into

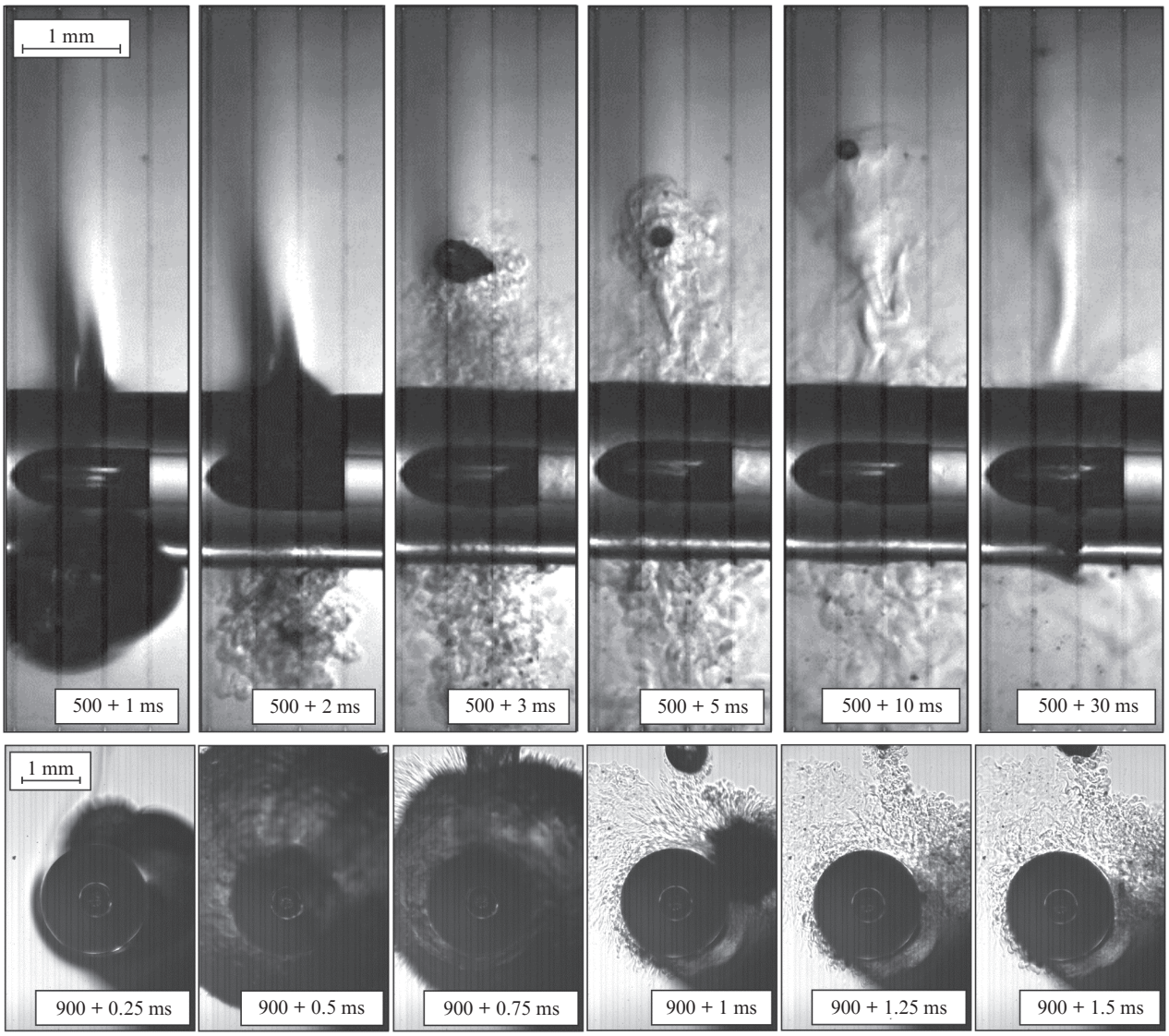

Figure 9. Dynamics of water heating through a radial-output fibre with laser radiation with λ= 1.94 μm and P = 5 W. An event of explosive boiling (the upper row is a profile view, and the lower one is a full-face view).

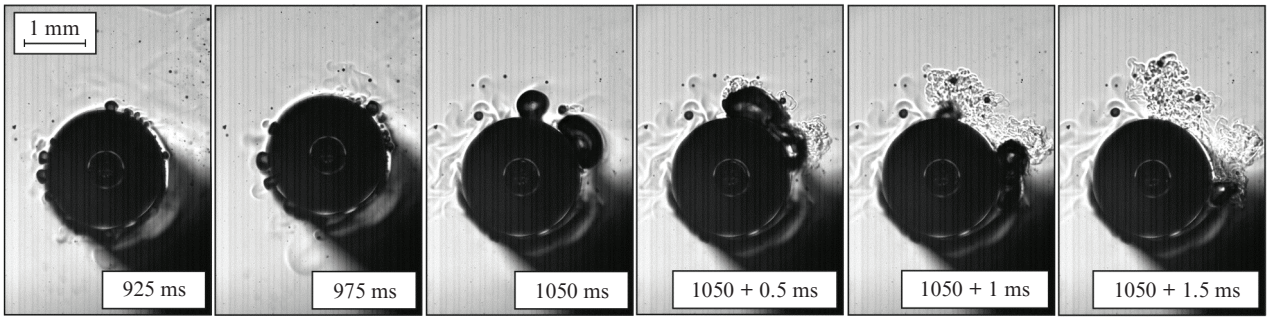

Figure 10. Dynamics of water heating through a radial-output fibre with laser radiation with λ = 1.94 μm and P = 5 W. Fine-bubble boiling between the events of explosive boiling (full-face view).

account the radiation scattering. Figure 12 shows the spectral dependences of the absorption coefficients μ_a for water and blood and the effective attenuation μ_{eff} for blood [11].

The characteristic thicknesses of the layers of water and blood in which radiation with wavelengths λ = 1.55 and 1.94 μm is absorbed can be determined as $d = \mu_a^{-1}$ and μ_{eff}^{-1}, respectively. For water, at λ = 1.55 μm, $\mu_a \approx 1$ mm^{-1} and $d \approx$ 1 mm, and at λ = 1.94 μm, $\mu_a \approx 13$ mm^{-1} and $d \approx 0.08$ mm. For blood at λ = 1.55 μm $\mu_{eff} \approx 3$ mm^{-1}, $d_f \approx 0.3$ mm, and at λ = 1.94 μm $\mu_{eff} \approx 28$ mm^{-1}, $d \approx 0.036$ mm.

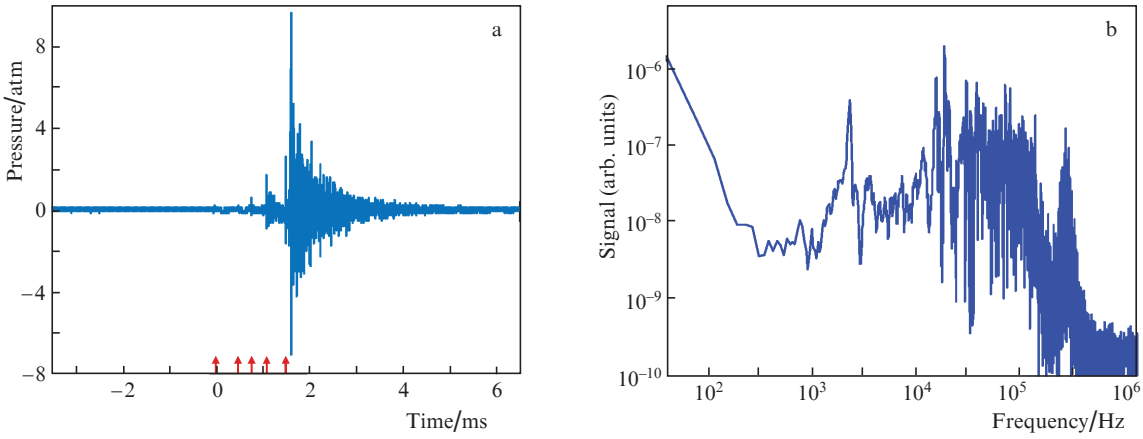

Figure 11. (a) Acoustic signal and (b) its spectrum during the first event of explosive boiling of water (radial-output fibre, $\lambda = 1.94$ μm, $P = 5$ W). The arrows indicate the acoustic pulses preceding the main burst.

Since the absorption in the blood is determined mainly by water (Fig. 12), before the onset of coagulation of the organic components of the blood, processes in water can model laser-induced processes in EVLC. It should be noted that the above estimates are valid in the absence of the Moses effect [12], when, due to super-intense boiling, a gas-vapour bubble is formed at the radiation exit point, the contents of which practically do not absorb laser radiation.

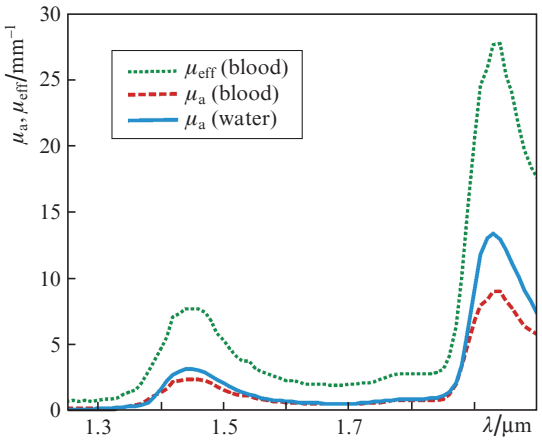

Figure 12. Spectral dependences of the coefficients of absorption μ_a and effective attenuation μ_{eff} in the erythrocyte emulsion (blood model with haematocrit Hct = 33.2%), as well as the absorption coefficient μ_a in water.

Analysis of shadow photographs shows that when using a fibre with an end-face output of radiation and $\lambda = 1.55$ μm (see Figs 2–4), the heat transfer at the initial stage is determined exclusively by convection. We believe that the apparent asymmetry observed in the frames, when the initial gradient structure forms near the lower part of the fibre, is associated with the occurrence of natural convection only in the upper part of the heated area. In the lower part, a heated, and therefore less dense, medium borders on a denser one; therefore, natural convective flows do not arise here.

Convective motions are known to prevail over other heat transfer processes if the buoyancy effects caused by a decrease in water density due to heating dominate viscous friction and thermal conductivity. These effects are determined by the Archimedes force acting on the volume of water with a characteristic size L: $F_A = \beta \Delta T \rho L^3 g$, where β is the temperature coefficient of volume expansion; ΔT is the temperature jump; ρ is the density of water; and g is the acceleration of gravity. The convection velocity V can be estimated by equating the Archimedes force to the Stokes viscous friction force $\rho \nu L V$, where ν is the kinematic viscosity:

$$V = \beta \Delta T L^2 g / \nu. \quad (1)$$

For intense convection, it is necessary that the characteristic ascent time, estimated as L/V, be much shorter than the characteristic temperature equalisation time, defined as L^2/α, where α is the thermal diffusivity of water, i.e., the Rayleigh number

$$\mathrm{Ra} = \frac{\beta \Delta T L^3 g}{\nu \alpha} \gg 1. \quad (2)$$

Substituting the tabular values for water ($\beta = 2 \times 10^{-4}$ K^{-1}, $\nu = 10^{-6}$ m^2 s^{-1}, $\alpha = 1.4 \times 10^{-7}$ m^2 s^{-1}) into Eqn (2), we find that for a characteristic size of the water volume $L = d = 1$ mm at $\lambda = 1.55$ μm, even in the case of a very small temperature jump ($\Delta T = 1$ K), intense convection will occur in the water (Ra ≈ 11).

Knowing the convective transfer rate, one can estimate the characteristic values of the average temperature heating near the end face of the fibre. It follows from Eqn (1) that for $V = 16$ mm s^{-1} (Fig. 2, $\lambda = 1.55$ μm, $P = 5$ W), the temperature jump in the heated volume $L^3 = 1$ mm^3 should be ~11 K, and for V = 20 mm s^{-1} (Fig. 3, $\lambda = 1.55$ μm, $P = 12$ W), $\Delta T \approx 14$ K.

Note that the obtained estimates of ΔT characterise the average values, and the maximum temperatures, as is well known, arise near the end of the fibre. The shape of the thermal front profiles in Figs 2–4 also indicates this, according to Eqn (2). Experiments have shown that in these areas a significant overheating of water can occur, accompanied by its explosive boiling with the formation and collapse of a gas-vapour (gas previously dissolved in water) macrobubble, the maximum diameter of which at $\lambda = 1.55$ μm and $P = 12$ W is about 5 mm (see Fig. 3). The macrobubble collapses in a time of ~250 μs, after which two-phase jets directed from the end arise, in which multiple microbubbles are observed.

We believe that the emergence of a macrobubble after the collapse (Fig. 3) of a long-lived bubble is associated with the known effect of the migration of bubbles towards a warmer area. This effect is explained by the appearance of Marangoni convection in the nonuniformly heated area, which arises due to the temperature dependence of the surface tension coefficient of water [13, 14]. When using distilled water, microbubbles migrating to the end face of the fibre actively capture various inclusions from the water and transfer them to the end face of the fibre [14].

The studies showed that, when proceeding to radiation with $\lambda = 1.94$ μm (Figs 5 and 6), the pattern of heat transfer changes: vivid convective heat transfer patterns observed at the initial stages of heating for $\lambda = 1.55$ μm are absent, and explosive boiling occurs at much lower powers. These changes can be explained by a significantly stronger absorption of laser radiation in water, which leads to heating of a very thin ($d \approx 80$ μm) layer near the fibre end face. In this case, the convective flow velocity will be significantly lower due to the proximity of the solid surface, and overheating will occur faster and at lower powers. Note that at higher radiation powers with strong absorption, an elongated pulsating vapour-gas macrobubble forms near the fibre end face, at the distal end of which a two-phase jet forms consisting of heated water and vapour-gas microbubbles [15].

Replacing an end-face output fibre with a radial output one (Figs 7–10), expectedly causes significant changes in the heat transfer pattern. A ring-shaped heated region appears around the fibre at the exit point of the laser radiation and upward convection occurs (Figs 7 and 8). Thus, gravity breaks heat transfer symmetry with respect to the axis of the fibre, which contradicts the basic assumptions underlying mathematical simulations, e.g., in Ref. [7].

For radial output, due to emitting area significantly larger than that of the fibre end face, the radiation power density is lower at the same P value. Accordingly, the thresholds for the power of development of the same hydrodynamic processes increase. Thus, for $\lambda = 1.55$ μm in the case of a radially emitting fibre in the entire range of studied powers (up to 15 W), no explosive boiling events were detected, and for $\lambda = 1.94$ μm they occurred at higher powers (see Fig. 9). An analysis of explosive boiling near a radially emitting fibre using high-speed images (a fragment in Fig. 9) showed that a chain of 'explosions' occurs during one to several milliseconds, which usually begins near the bottom of the fibre. The results obtained by recording an acoustic signal also confirm this observation. It can be seen from Fig. 11a that before the main burst a whole chain of short pulse signals is observed, among which, obviously, there are no repeated reflections, since their maximum amplitudes gradually increase with time. These signals, together with the main burst, form the broadband spectrum of the acoustic signal (Fig. 11, b).

We believe that the results obtained in water qualitatively simulate the processes that occur when using optical fibres with end-face and radial output in a clinic with endovenous laser coagulation before the coagulation of organic blood components begins.

5. Conclusions

We report experimental modelling of laser-induced hydrodynamic processes occurring in the blood with EVLC. The study was conducted in the aquatic environment using high-speed video recording with the registration of the heating process by the shadow optical method. It is shown that in the case of laser radiation that is strongly absorbed in water, convection and boiling play the main role in the process of heat transfer. In this case, the boiling can be fine-bubble or explosive and can be accompanied by the formation of two-phase jets. This fact shows the failure of mathematical models considering heat transfer due to heat conduction. It is shown that effective heat transfer when using radiation with $\lambda = 1.94$ μm begins at significantly lower power levels compared with radiation with $\lambda = 1.55$ μm. This circumstance indicates the possibility of reducing the radiation power, providing the required efficiency of EVLC.

It was found that the heat transfer is sharply asymmetric and directed mainly upward and forward (when output through the end face) or upward (when output radially). Thus, uniformity of the thermal damage to the vein wall during EVLC is achievable only when the vein is crimped under the influence of tumescent anaesthesia and its wall contacts the surface of the radial-output fibre.

Acknowledgements. This work was supported by the Ministry of Science and Higher Education as part of the fulfilment of the State Assignment of the Federal Research Centre for Crystallography and Photonics of the Russian Academy of Sciences (development of laser technologies) and by the Russian Foundation for Basic Research (Project No. 18-29-06056, studying the explosive boiling process).

References

1. Sokolov A.L. et al. *Lazernaya obliteratsiya ven dlya prakticheskikh vrachey* (Laser Obliteration of Veins for Practitioners) (Moscow: ID 'Medpraktika-M', 2011).
2. Krochek I.V. et al. *UZI-kontroliruemaya vnutripolostnaya lazernaya obliteratsiya kist. Uchebnoe posobie* (Ultrasound-Controlled Intracavity Laser Obliteration of Cysts. Study Guide) (Chelyabinsk: Titul, 2016).
3. Mordon S.R., Wassmer B., Zemmouri J. *Lasers in Surgery and Medicine*, **39**, 256 (2007).
4. Ignatieva N.Yu. et al. *Lasers Med. Sci.*, **32**, 1105 (2017). DOI: 10.1007/s10103-017-2214-x.
5. Poluektova A.A. et al. *Lasers Med. Sci.*, **29**, 441 (2014). DOI: 10.1007/s10103-013-1450-y.
6. Artemov S.A. et al. *Lasers Med. Sci.*, **35**, 867 (2020). DOI: 10.1007/s10103-019-02874-6.
7. Artemov S.A. et al. *Proc. Conf. "Advanced Laser Technologies"* (Prague, 2019) B-O-10.
8. Disselhoff B.C. et al. *Phlebology*, **23**, 69 (2008). DOI: 10.1258/phleb.2007.007038.
9. Chudnovsky V.M. et al. *Quantum Electron.*, **47** (4), 361 (2017) [*Kvantovaya Elektron.*, **47** (4), 361 (2017)].
10. Chudnovskii V. et al. *Lasers Med. Sci.*, **33** (8), 1821 (2018). DOI: 10.1007/s10103-018-2552-3.
11. Marchenko A.A. et al. *Lazernaya Meditsina*, **23** (2), 44 (2019).
12. Elhilali M.M. et al. *J. Endourology*, **31** (6), 598 (2017).
13. Ortega-Mendoza J.G. et al. *Opt. Express*, **26** (6), 6653 (2018).
14. Yusupov V.I., Tsypina S.I., Bagratashvili V.N. *Laser Phys. Lett.*, **11** (11), 116001 (2014).
15. Minaev V.P. et al. *Quantum Electron.*, **49** (4), 404 (2019) [*Kvantovaya Elektron.*, **49** (4), 404 (2019)].